TECHNICAL ARTICLE

X-ray investigations into silica/silver nanocomposite

K. Dudek,[1,a)] J. Podwórny,[1] M. Dulski,[2] A. Nowak,[3] and J. Peszke[3]
[1]*Refractory Materials Division in Gliwice, Institute of Ceramics and Building Materials, Gliwice, Poland*
[2]*Institute of Material Science, University of Silesia, Chorzow, Poland*
[3]*A. Chelkowski Institute of Physics, University of Silesia, Katowice, Poland*

(Received 26 September 2016; accepted 6 February 2017)

X-ray diffraction data revealed that the initial SiO_2/Ag nanocomposite, manufactured in a chemical synthesis process, is mainly composed of silica in amorphous phase (95.5 wt.%), crystalline Ag with a cubic structure (*Fm*-3*m*) and cristobalite (SiO_2) with a tetragonal structure ($P4_12_12$) in the amount of 4.2 and 0.3 wt.%, respectively. High-temperature diffraction data revealed high stability of the SiO_2/Ag composite up to 1000 °C. High-temperature X-ray diffraction measurements revealed phase cristallization temperatures of silica at 1060 °C for cristobalite and 1080 °C for tridymite as well as temperature of silver evaporation starting from the composite (ca. 1000 °C). Infrared spectroscopy data confirmed the presence of amorphous matrix with embedded silver ions and crystalline compounds in the form of cristobalite and tridymite without silver after thermal treatment. © *2017 International Centre for Diffraction Data.* [doi:10.1017/S0885715617000185]

Key words: silica–silver (SiO_2/Ag) nanocomposite, amorphous phase, silica phase transitions

I. INTRODUCTION

Metallic nanoparticles (NPs), such as Au, Pt, Zn, Cu (Revina *et al.*, 2007; Chaloupka *et al.*, 2010; Sotiriou and Pratsinis, 2010; Cioffi and Rai, 2012; Aguilar, 2013), and their nanocomposites (such as nanometallic-doped ceramics or polymers), especially silver in nanometer size (nAg) (Gong *et al.*, 2007; Baheiraei *et al.*, 2012; Dong *et al.*, 2014; Nowak *et al.*, 2016) are very attractive materials for medical application because of their bactericide features.

Bacterial infections are a major problem after implantation and can result in the rejection of implants. Therefore, it is reasonable to ensure the antibacterial activity of implantation materials. This aim is achieved by modifying the surface of implants with antibiotics or silver particles in the nanometer size (nAg). It turns out that nanosilver and antibiotics have a similar effect on microorganisms. However, microorganisms do not become resistant to silver. Thus, silver is a one of the most effective elements which can be applied against 99.9% of bacteria and fungi (Chaloupka *et al.*, 2010; Sotiriou and Pratsinis, 2010; Aguilar, 2013). It can also be successfully used as an individual element in the production of protective coatings and help to develop innovative multifunctional composites.

Silica is a biocompatible, non-toxic material, which does not cause allergy. It has good adhesive properties and a potential to create chemical bonds with metallic substrates. In addition, silica matrix enables incorporation of metal ions (e.g. silver) in low concentrations and their gradual release into the environment, which will provide a long-lasting antibacterial effect (Gong *et al.*, 2007; Baheiraei *et al.*, 2012; Aguilar, 2013; Dong *et al.*, 2014). Therefore, a composite system in such a form may be used as a material for preparing multifunctional layers.

Quality, structure, chemical composition, morphology, and surface topography are also very important for the implant acceptance in the organism and metabolic processes of surrounding tissues. The quality of coatings depends on the applied surface modification technique and the quality of the starting materials. The applied surface engineering method affects the microstructure, porosity, adhesion force, morphology, and topography of the coatings. Most of these techniques require elevated temperatures or post-sintering treatment (Dickerson and Boccacini, 2012; Dudek and Goryczka, 2016), which results in structural changes of materials and significantly affects their crucial properties. Therefore, it is very important to carry out a detailed characterization of structural changes during heat treatment for every novel material.

The main goal of this paper is to determine optimal temperature conditions, which allow preserving structural and physicochemical properties of SiO_2/Ag nanocomposite. For this purpose, high-temperature X-ray diffraction (HT-XRD) measurements were carried out so as to correlate the temperature effect with structural changes of the material. The characteristics of initial silica–silver nanocomposite powder before and after heat treatment were analyzed using XRD, infrared spectroscopy, and scanning electron microscopy/energy dispersive spectrometer (SEM/EDS) microscopy.

II. MATERIAL AND METHOD

Silicon dioxide/silver nanocomposite was synthesized by a chemical reaction method. The starting materials were silicon dioxide, potassium hydroxide, nitric acid, ammonia, and silver acetate. All used chemicals were of analytical grade and commercially available. First, the silicon dioxide was mixed with 50 ml distilled water in the ratio 1:5, respectively and 0.2 ml potassium hydroxide with 0.01 ml of ammonia. To the colloid suspension was added dropwise 10 ml of 4% silver acetate water solution. Then to stirred colloid solution was put 0.02 ml of concentrate nitric acid. Finally, the system was filtered on a polyethylene filter, washed, and dried at room temperature.

[a)]Author to whom correspondence should be addressed. Electronic mail: k.dudek@icimb.pl

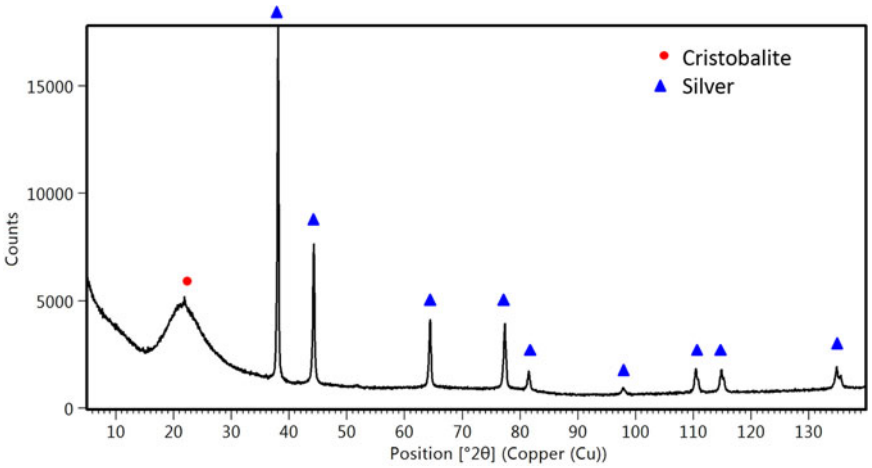

Figure 1. XRD pattern collected at ambient temperature for SiO_2/Ag powder.

The structure of the material was investigated by an X'PertPro MPD PANalytical X-ray diffractometer with a CuK_α tube. The content of amorphous phase for the initial SiO_2/Ag powder was determined using 15 wt.% crystalline quartz (SiO_2) as an internal standard (Gualtieri, 1999). HT-XRD measurements were performed at a temperature ranging from 25 to 1200 °C with a heating/cooling rate of 10/30 °C per minute, using a high-temperature chamber Anton Paar HTK 2000. The sample was placed on a 1 mm-thick c-ZrO_2 protective plate to prevent chemical reactions of Ag with the Pt heating stripe at elevated temperatures. The protective plate material was inert in the tested system. XRD patterns were collected every 20° with 5 min soaking. The quantitative phase analyses and lattice parameters were refined by the Rietveld method (Rietveld, 1969) with HighScore Plus software. The silver content was determined from the net area of silver diffraction line (111) at $2\theta =$ 38.085° collected at low temperatures.

Infrared (IR) measurements were carried out using an Agilent Cary 640 FTIR spectrometer equipped with a standard source and a DTGS Peltier-cooled detector. The spectra were collected at room temperature using GladiATR diamond equipment (Pike Technologies) within 4000–400 cm^{-1} range. All the spectra were collected before and after thermal treatment with a spectral resolution of 4 cm^{-1} and recorded in the form of 16 scans. The baseline correction was done and water vapor and carbon dioxide was subtracted from each spectrum.

SEM data were obtained by TESCAN Mira 3 LMU equipped with an EDS from Oxford Instruments – Aztek. Images were collected by secondary electrons and backscattered electrons (BSE). The measurements were carried out on the samples covered by 5 nm of Cr layer by using Quorum Q150T ES equipment.

III. RESULTS AND DISCUSSION

A. Initial material

The results of determining the phase composition of SiO_2/Ag nanocomposite are illustrated in Figure 1. The XRD measurements carried out for the powder material showed its crystalline and amorphous state. Strong and sharp diffraction lines originate mainly from silver (Ag) with a cubic structure (Fm-3m) "PDF 04-004-6434 (ICDD, 2015)" and, to a lesser extent, from cristobalite (SiO_2) with a tetragonal structure ($P4_12_12$) "PDF 04-007-5018 (ICDD, 2015)". Thus, the lattice parameters based on the Rietveld refinement for silver are determined as $a_0 = 4086(9)$ Å, while for cristobalite as $a_0 = 5.195(2)$ and $c_0 = 6.465(7)$ Å. Quantitative analysis of SiO_2/Ag nanosystems allows finding the percentage amount of crystalline silver, cristobalite and amorphous phases in the whole volume as 4.2(1), 0.3(2), and 95.5(1)%, respectively. Satisfactory values of agreement indices $R_{exp} = 2.13$, $R_{wt} =$ 6.73%, and GoF = 3.16 were achieved.

The IR spectrum of the initial SiO_2/Ag nanocomposite is presented in Figure 2. The spectrum is dominated by three absorption bands centered in the 400–1300 cm^{-1} region, ascribed to Si–O–Si vibrations (Ramalingam *et al.*, 2014). In more detail, the deconvolution procedure points to the presence of bands centered at 960, 981 cm^{-1}, which originate from the Si–OH bond (Ramalingam *et al.*, 2014), structural deformation within the silica network or non-stoichiometric silicon oxide (Zhao *et al.*, 2011). The Si–O–Si band separation (445 cm^{-1} pure silica = 417 + 458 cm^{-1}) suggests the silica network deformation as well as the formation of an outer polymeric cage within the silica network (Shameema *et al.*, 2006; Ramalingam *et al.*, 2014). Additionally, weak bands located at ca. 1500 cm^{-1} might be ascribed to the presence of silver, while the bands between 1650 and 1750 cm^{-1} to the stretching vibration of υ(C=O) from the aldehyde group and/or

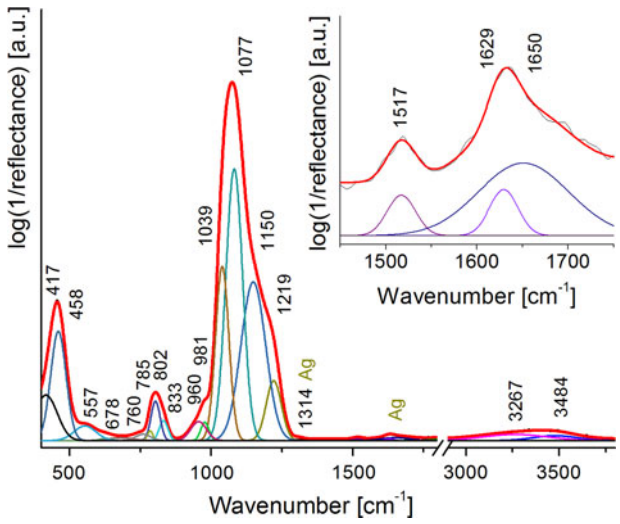

Figure 2. IR spectra of SiO_2/Ag nanocomposite fitted by Voigt curves in the 400–3800 cm^{-1} range. Magnified region ranged between 1450 and 1750 cm^{-1} summarizes a potential region of silver occurrence.

https://doi.org/10.1017/S0885715617000185 Published online by Cambridge University Press

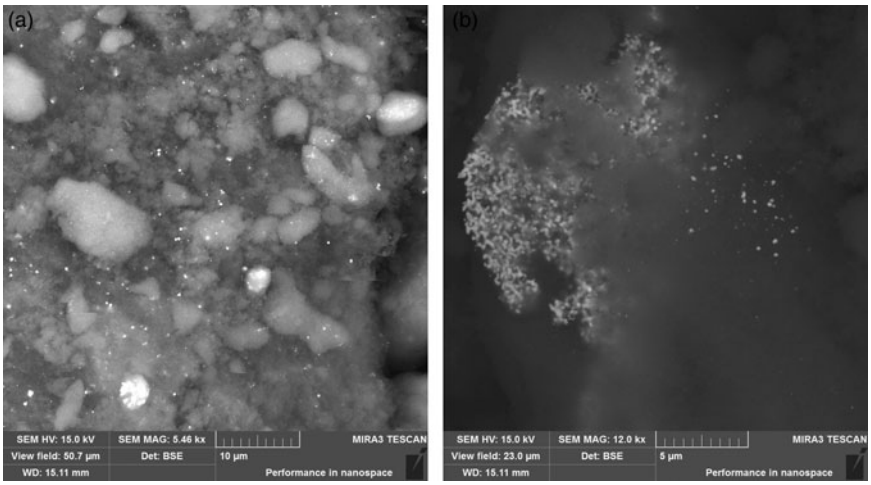

Figure 3. BSE–SEM image of SiO_2/Ag composite.

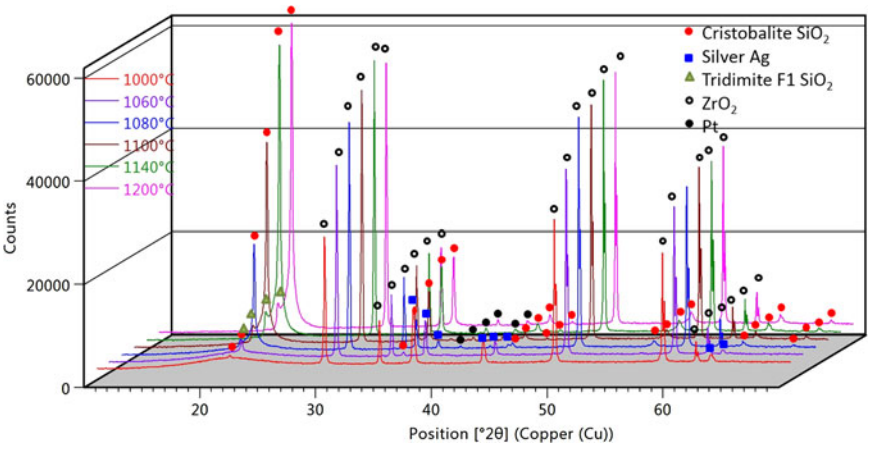

Figure 4. HT-XRD patterns for SiO_2/Ag composite measured from 1000 to 1200 °C.

the deformational mode of water molecule. In the high wavenumber region (3200–3800 cm^{-1}), the bands originate from the stretching mode of υ(Si–OH), υ(OH) as well as molecular water [υ(H–O–H)] adsorbed on the silica surface (Moghanian *et al.*, 2014; Ramalingam *et al.*, 2014). The presence of hydroxyl groups might also be because of hydroxyl ions over the Ag NPs. The aldehyde and polymeric groups might originate from substrates used in the manufacturing process of SiO_2/Ag nanocomposite.

BSE–SEM image of SiO_2/Ag nanocomposite is presented in Figure 3. Microscopic observations combined with an EDS analysis revealed the occurrence of silica in nanometer size with a tendency to agglomerate in higher aggregates (gray areas in Figure 3). Moreover, brighter areas in Figure 3 result from the presence of silver in the silica matrix in two forms – homogenously distributed NPs [Figure 3(a)] and its agglomerates [Figure 3(b)]. The size of silver particles estimated on the basis of SEM images was found to vary from a few nanometers to even ca. 300 nm.

B. Structural changes of SiO_2/Ag composite at high temperatures

HT-XRD patterns recorded for SiO_2/Ag composite show no phase transformations during temperature alterations up to 1000 °C. It is especially well visible in an analysis of the intensity and net area of the peak (101) at $2\theta = 21.916°$ of cristobalite and background level characteristic of amorphous phase, which remain unchanged during the sample heating. The XRD patterns revealed only a slight shift of diffraction lines caused by the material's thermal expansion. However, there were no signs of amorphous silica crystallization. HT-XRD data presented in Figure 4 revealed the initial stage of crystallization of amorphous silica above 1040° toward the high-temperature type of cristobalite with a cubic structure (*Fd*-3*m*) "PDF-04-007-5021 (ICDD, 2015)". The most intensive crystallization effect was found in the temperature range of from 1080 to 1120 °C. Above

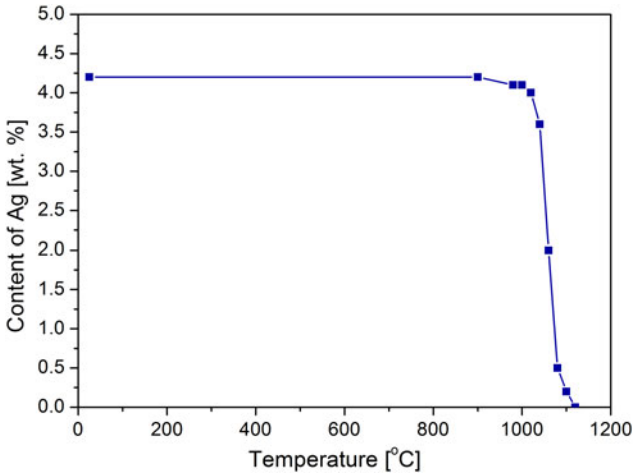

Figure 5. Changes in Ag content determined from HT-XRD data.

https://doi.org/10.1017/S0885715617000185 Published online by Cambridge University Press

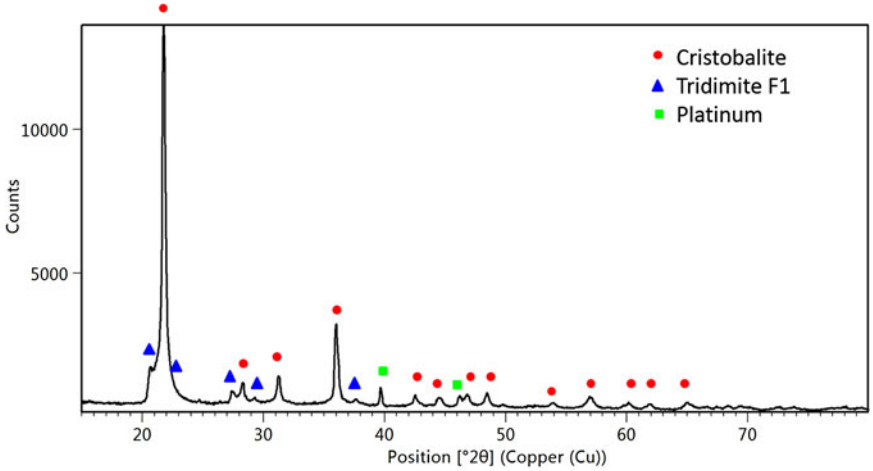

Figure 6. IR spectra of SiO_2/Ag nanocomposite after heat treatment fitted by Voigt curves in the 400–3800 cm^{-1} range. Magnified region ranged between 1750 and 1450 cm^{-1} summarizes the presence of a region of potential silver occurrence.

1140 °C no difference in the intensity of reflections belonging to cristobalite was visible. Additionally, at temperatures above 1080 °C the appearance of diffraction lines from tridymite (SiO_2) with a disordered anorthic $F1$ structure was observed "PDF 01-071-0261 (ICDD, 2015)". Their intensities increase up to 1140 °C and then remain unchanged. Diffraction data also revealed a decrease in the background level characteristic of amorphous phase up to 1140 °C. As a result, above 1140° the material is mainly composed by crystalline silica phases.

It is noteworthy that because of high-temperature experiments and the necessity to use a protective plate holder, additional diffraction lines originating from ZrO_2 with a cubic structure (Fm-3m) "PDF 04-005-9865 (ICDD, 2015)" were observed. Furthermore, evaporation of platinum from the heating stripe at 1080 °C results in its depositing on the composite surface and generates additional diffraction lines from crystalline platinum (Pt) with a cubic structure (Fm-3m) "PDF 04-003-7036 (ICDD, 2015)".

Finally, XRD results revealed a decrease of the net area and intensities of diffraction lines belonging to the crystalline silver because of Ag evaporation from the composite (Figure 5). Interestingly, the silver concentration estimated on the basis of XRD results is not affected by temperature changes even up to 900 °C. In the temperature range of 900–1000 °C, a slight decrease in the intensity of silver diffraction lines corresponds to a decrease of silver amount from 4.2 to 4.1%, whereas 89% of Ag evaporates from the composite at temperatures between 1060 and 1080 °C. Above 1110 °C silver was no longer detectable by the X-ray method.

C. Material after heat treatment

XRD pattern of the composite after tests revealed the presence of cristobalite (SiO_2) with a tetragonal structure ($P4_12_12$) "PDF 04-007-5018 (ICDD, 2015)" and tridymite with the $F1$ structure "PDF 01-071-0261 (ICDD, 2015)". Some distortion of the right side of the main diffraction line of cristobalite (101) at $2\theta = 21.916°$ and an unclearly visible weak and broad peak of the left side, belonging to tridymite, might indicate a poorly-crystallized anorthic $F1$ tridymite structure. According to the ICCD data, the lattice parameters of that phase are as followed: $a_0 = 9.9320$, $b_0 = 17.2160$, and $c_0 = 81.8640$ Å. Such a large size of the unit cell leads to disorder in the structure of tridymite and results in distortions of diffraction lines in the X-ray patterns.

Moreover, there are no diffraction lines belonging to silver. Platinum with a cubic structure (Fm-3m) "PDF 04-003-7036 (ICDD, 2015)" occurred as a consequence of evaporation from the heating stripe and deposition of the investigated material on the surface. The positions of platinum diffraction lines indicate no chemical reactions between the composite material and Pt ions.

The IR spectrum of SiO_2/Ag after heat treatment is presented in Figure 6. The deconvolution procedure and peak fitting analysis revealed only the presence of typical Si–O–Si (750–1300 cm^{-1}) and O–Si–O (350–750 cm^{-1}) vibrations as well as the lack of silver, hydroxyl, and polymer bands. Moreover, the band position (445 cm^{-1}) confirmed the metal-free silica structure. A more detailed analysis revealed cristobalite bands centered at 509, 620, 790, and 1094 cm^{-1} (Sitarz *et al.*, 2000; Liang *et al.*, 2006; Koike *et al.*, 2013) and tridymite ones located at 435, 476, 778, 1005, and 1157 cm^{-1} (Wilson *et al.*, 1974; Sitarz *et al.*, 2000). The location of other bands is probably associated with structural deformation within the silica network, which is confirmed by X-ray measurements (Figure 7).

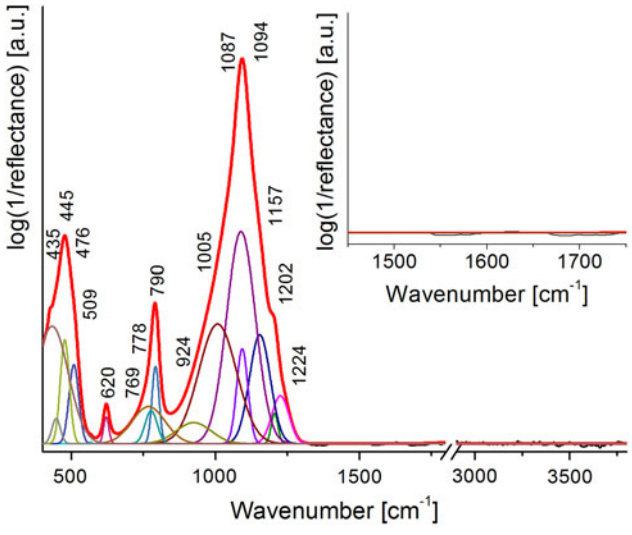

Figure 7. XRD pattern recorded at ambient temperature for SiO_2/Ag powder after heat treatment.

https://doi.org/10.1017/S0885715617000185 Published online by Cambridge University Press

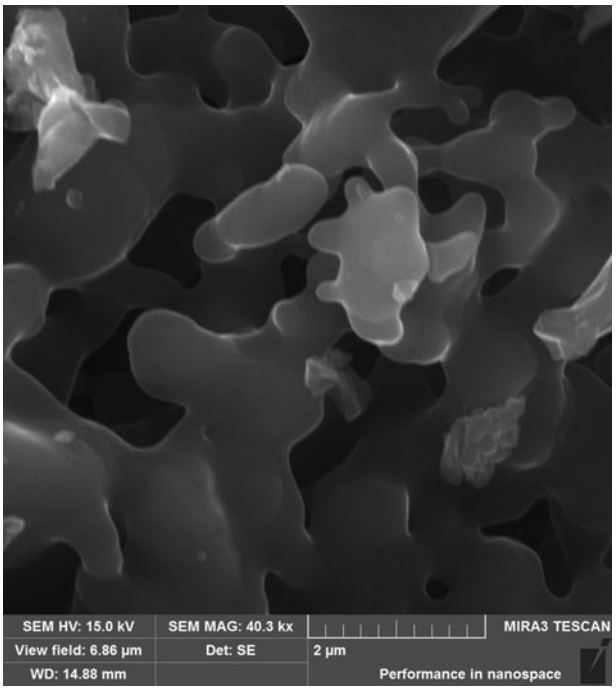

Figure 8. BSE–SEM image of the composite after heat treatment.

SEM studies revealed consolidation of silica NPs to irregular shapes and an increase of their size from nano- to micrometer's level (Figure 8). It should be noted that an increase of NPs size is an unfavorable effect, which may lead to changes of desirable material properties. The chemical composition of the tested composite after thermal treatment obtained from EDS analysis revealed the lack of signal from silver and the presence of silica and oxygen: the main elements of cristobalite and tridymite.

IV. CONCLUSIONS

XRD studies revealed that the structure of SiO_2/Ag composite was stable up to 1000 °C without clearly visible silver evaporation from the material. IR spectroscopy confirmed the predominant presence of amorphous phase in the composite and the presence of silver embedded into the silica matrix. HT-XRD measurements revealed the initiation of cristobalite crystallization from amorphous phase at 1060° and tridymite at 1080 °C. XRD and IR data revealed the presence of only two silica phases: cristobalite and tridymite after heat treatment. Moreover, the most of silver content was found to decrease above 1060 °C, whereas above 1110 °C silver in the sample was no longer detectable in the sample by X-ray (XRD), microscopy (SEM–EDS) or spectroscopy methods (IR). Finally, sintering of silica NPs and a significant increase of the particles size was observed. In order to preserve silver particles in the composite, the heat treatment temperature should not exceed 1000 °C.

Aguilar, Z. A. (**2013**). *Nanomaterials for Medical Applications* (Elsevier).

Baheiraei, N., Moztarzadeh, F., and Hedayati, M. (**2012**). "Preparation and antibacterial activity of Ag/SiO_2 thin film on glazed ceramic tiles by sol–gel method," Ceram. Int. **38**, 2921–2925.

Chaloupka, K., Malam, Y., and Seifalian, A. M. (**2010**). "Nanosilver as a new generation of nanoproduct in biomedical applications," Trends Biotechnol. **28**(11), 580–588.

Cioffi, N. and Rai, M. (**2012**). *Nano-Antimicrobials – Progress and Prospects* (Springer, Berlin–Heidelberg).

Dickerson, J. H. and Boccacini, A. R. (**2012**). *Electrophoretic Deposition of Nanomaterials* (Springer).

Dong, Y., Liu, T., Sun, S., Chang, X., and Guo, N. (**2014**). "Preparation and characterization of SiO_2/polydopamine/Ag nanocomposites with long-term antibacterial activity," Ceram. Int. **40**(5), 605–5609.

Dudek, K. and Goryczka, T. (**2016**). "Electrophoretic deposition and characterization of thin hydroxyapatite coatings formed on the surface of NiTi shape memory alloy," Ceram. Int. **42**(16), 19124–19132.

Gong, J., Liang, Y., Huang, Y., Chen, J., Jiang, J., Shen, G., and Yu, R. (**2007**). "Ag/SiO_2 core-shell nanoparticle-based surface-enhanced Raman probes for immunoassay of cancer marker using silica-coated magnetic nanoparticles as separation tools", Biosens. Bioelectron. **22**, 1501–1507.

Gualtieri, A. F. (**1999**). "Accuracy of XRPD QPA using the combined Rietveld – RIR method", J. Appl. Crystallogr. **33**, 267–278.

ICDD (**2015**). PDF-4+ 2015 (Database), edited by Dr. Soorya Kabekkodu, International Centre for Diffraction Data, Newton Square, PA, USA.

Koike, G. C., Noguchi, R., Chihara, H., Suto, H., Ohtaka, O., Imai, Y., Matsumoto, T., and Tsuchiyama, A. (**2013**). "Infrared spectra of silica polymorphs and the conditions of their formation", Astrophys. J. **778**, 1.

Liang, Y., Miranda, C., and Scandolo, S. (**2006**). "Infrared and Raman spectra of silica polymorphs from an ab initio parametrized polarizable force field," J. Chem. Phys. **125**(19), 194524.

Moghanian, H., Mobinikhaledi, A., Blackmanc, A. G., and Sarough-Farahani, E. (**2014**). "Sulfanilic acid-functionalized silica-coated magnetite nanoparticles as an efficient, reusable and magnetically separable catalyst for the solventfree synthesis of 1-amido- and 1-aminoalkyl-2-naphthols," RSC Adv. **4**, 28176–28185.

Nowak, A., Szade, J., Talik, E., Zubko, M., Wasilkowski, D., Dulski, M., Balin, K., Mrozik, A., and Peszke, J. (**2016**). "Physicochemical and antibacterial characterization of ionocity Ag/Cu powder nanoparticles," Mater. Charact. **117**, 9–16.

Ramalingam, S., Devi, L. B., Rao, J., and Nair, B. U. (**2014**). "Rapid hydrogenation: perfect quasi architecture (Ag@SiO_2NPs) as a substrate for nitrophenol reduction," RSC Adv. **4**, 56041–56051.

Revina, A. A., Oksentyuk, E. V., and Fenin, A. A. (**2007**). "Synthesis and properties of zinc nanoparticles: the role and prospects of radiation chemistry in the development of modern nanotechnology," Prot. Met. **43**, 554–559.

Rietveld, H. M. (**1969**). "A profile refinement method for nuclear and magnetic structures", J. Appl. Crystallogr. **2**, 65–71.

Shameema, O., Ramachandran, C. N., and Sathyamurthy, N. (**2006**). "Blue shift in X−H stretching frequency of molecules due to confinement," J. Phys. Chem. A **110**, 2–4.

Sitarz, M., Handke, M., and Mozgawa, W. (**2000**). "Identification of silicooxygen rings in SiO_2 based on IR spectra", Spectrochim. Acta A **56**(9), 1819–23.

Sotiriou, G. A. and Pratsinis, S. E. (**2010**). "Antibacterial activity of nanosilver ions and particles," Environ. Sci. Technol. **44**(14), 5649–5654.

Wilson, J., Russell, J. D., and Tait, J. M. (**1974**). "A new interpretation of the structure of disordered α-cristobalite," Contrib. Mineral. Petrol. **47**(1), 1–6.

Zhao, F., Wang, X., Ding, B., Lin, J., Hu, J., Si, Y., Yu, J., and Sun, G. (**2011**). "Nanoparticle decorated fibrous silica membranes exhibiting biomimetic superhydrophobicity and highly flexible properties," RSC Adv. **1**, 1482–1488.

https://doi.org/10.1017/S0885715617000185 Published online by Cambridge University Press